Society of Medical Education & Research

2024, Volume 4, Issue 1, Page No: 147-163
ISSN: 3108-4834

Archive of International Journal of Cancer and Allied Science

Circular RNA Hsa_circ_0136666 Drives Gastric Cancer Growth and Immune Escape through miR-375/PRKDC-Mediated PD-L1 Phosphorylation

Natalia Sofia Alvarez[1]*, Camila Beatriz Rojas[1]

[1]Department of Oncology, Universidad de Chile Clinical Hospital, Santiago, Chile.

***E-mail** ✉ n.alvarez.uc@gmail.com

Abstract

The effectiveness of targeted therapies in prolonging survival for gastric cancer patients remains limited, largely due to off-target effects and tumor immune evasion. Circular RNAs (circRNAs) are abundant in tumor tissues and serve as potential biomarkers and therapeutic targets. The role of hsa_circ_0136666 in promoting gastric cancer cell proliferation was examined using Western blot, qRT-PCR, fluorescence in situ hybridization (FISH), and flow cytometry. Tumor immune evasion was investigated in tumor-bearing mice through tissue immunofluorescence, enzyme-linked immunosorbent assay (ELISA), and flow cytometric analysis. Expression differences of circRNAs in clinical samples were assessed using tissue microarray FISH. The impact of siRNA on enhancing anti-PD-L1 therapy and modulating the tumor immune microenvironment was evaluated in a coadministration model. Hsa_circ_0136666 was highly expressed in gastric cancer tissues and cell lines. Functionally, it promoted tumor proliferation and shaped the tumor microenvironment, facilitating immune escape in a CD8+ T cell-dependent manner. Mechanistically, hsa_circ_0136666 acted as a sponge for miR-375-3p, thereby upregulating PRKDC, modulating immune checkpoint proteins, and promoting PD-L1 phosphorylation to prevent its degradation. This process induced PD-L1 aggregation and suppressed immune activity, impairing anti-tumor immune responses. Therapeutically, LNP-siRNA targeting hsa_circ_0136666 enhanced the efficacy of anti-PD-L1 treatment and reduced immune evasion. These findings identify hsa_circ_0136666 as an oncogenic circRNA in gastric cancer that drives PD-L1 phosphorylation through the miR-375/PRKDC axis, promoting immune escape. This study uncovers a novel pathogenic mechanism, highlights hsa_circ_0136666 as a potential immunotherapeutic target, and provides a rationale for improving anti-PD-L1 therapy in gastric cancer.

Keywords: miR-375, PD-L1, Circular RNA, Immune escape, Gastric cancer

Introduction

Gastric cancer (GC) represents a major public health challenge worldwide, with high incidence and mortality rates in many regions. The disease accounts for more than 700,000 deaths annually, ranking it as the third leading cause of cancer-related mortality globally [1]. Clinical symptoms typically appear only at advanced stages, complicating early diagnosis [2, 3]. Moreover, current therapeutic strategies are limited by patient health status, tumor drug resistance, and treatment-related side effects, failing to achieve the desired outcomes [4]. Consequently, the identification of reliable early diagnostic biomarkers and the development of effective therapeutic approaches for GC remain urgent priorities.

Circular RNAs (circRNAs) are highly conserved non-coding RNAs characterized by covalently closed-loop structures [5, 6]. Functionally, circRNAs can act as miRNA sponges, transcriptional regulators, or interact with RNA-binding proteins, and some can even encode functional peptides [7]. Accumulating evidence has linked circRNAs to a range of diseases, including diabetes, neurological disorders, cardiovascular diseases, and cancers [8, 9]. In particular, circRNAs are increasingly recognized as important regulators in gastric carcinogenesis [10, 11], where they modulate gene

Access this article online https://smerpub.com/

Received: 02 February 2024; **Accepted:** 15 May 2024

How to cite this article: Alvarez NS, Rojas CB. Circular RNA Hsa circ 0136666 Drives Gastric Cancer Growth and Immune Escape through miR-375/PRKDC-Mediated PD-L1 Phosphorylation. Arch Int J Cancer Allied Sci. 2024;4(1):147-63. https://doi.org/10.51847/KvrZUdLZyV

expression by competitively binding to miRNA response elements and sequestering microRNAs (miRNAs) [12].

MiRNAs are another class of abundant non-coding RNAs that bind target mRNAs, leading to their degradation and regulating diverse biological processes [13]. Previous studies, including our own, have shown that miR-375 is downregulated in gastric cancer and functions as a tumor suppressor [14, 15].

In this study, we focused on circPRKDC due to the critical role of PRKDC, the catalytic subunit of DNA-dependent protein kinase (DNA-PK), in DNA double-strand break repair and recombination [16]. PRKDC also acts as a protein kinase, phosphorylating multiple substrates to regulate their activity [17]. Immune checkpoint proteins, such as PD-L1, are subject to various post-translational modifications—including phosphorylation, palmitoylation, and ubiquitination—which influence tumor progression [18–22].

We demonstrate that hsa_circ_0136666 is highly expressed in gastric cancer and functions as a molecular sponge for miR-375. By sequestering miR-375, hsa_circ_0136666 upregulates PRKDC expression, which in turn phosphorylates and stabilizes PD-L1, thereby promoting gastric cancer progression and facilitating immune evasion.

Materials and Methods

Human tissue specimens

A total of 50 clinicopathological tissue samples were analyzed, including 21 cases of gastric cancer recurrence and metastasis (7 cases with primary tumor/adjacent tumor/metastasis, 5 cases with primary tumor/adjacent tumor, 5 cases with primary tumor/metastasis, and 4 cases of metastasis) and 5 cases of normal gastric mucosa. The study protocol was approved by the Ethics Committees of Shandong University, Taizhou Hospital, and Shanghai Outdo Biotech Company.

Cell culture and transfection

GES-1, MKN-45, and MFC cell lines were maintained in RPMI-1640 medium, whereas HEK-293T cells were grown in DMEM (KeyGEN, China). AGS cells were cultured in AGS-specific medium (Procell, CM-0022). All media were supplemented with 10% fetal bovine serum (FBS; LONSERA, Shanghai, China), and cells were incubated at 37 °C with 5% CO_2. All lines were sourced from the Cell Bank of the Chinese Academy of Sciences and used for experiments within 20 passages. Transfection of siRNAs, miRNA mimics, or plasmid constructs was carried out using jetPRIME® (Polyplus-transfection, New York, USA) in accordance with the manufacturer's instructions.

Transcription inhibition assay (actinomycin D treatment)

To assess RNA stability, cells were treated with 2 μg/mL actinomycin D (APExBIO, USA) or DMSO as a control for 2, 4, 8, and 12 hours. Levels of hsa_circ_0136666 and linear PRKDC transcripts were quantified via QRT-PCR at each time point.

RNase R treatment

One microgram of total RNA was incubated with or without RNase R (1 U/μg; Geenseed, Guangzhou, China) at 37 °C for 10 minutes. The treated RNA was reverse-transcribed into cDNA and analyzed by QRT-PCR to compare the resistance of circular versus linear transcripts.

RNA fluorescence in situ hybridization (FISH)

To visualize the localization of RNAs, Cy3-labeled probes targeting miR-375 and FITC-labeled probes for hsa_circ_0136666 and PRKDC mRNA were applied. Hybridization was performed on MKN-45 cells fixed in 4% paraformaldehyde. Cells were denatured at 73 °C for 5 minutes and incubated with probes overnight at 37 °C in darkness using the RNA-FISH kit (GenePharma). Fluorescence images were captured with a confocal laser scanning microscope and analyzed using CaseViewer software.

RNA extraction and quantitative PCR

Total RNA was isolated from cells and tissue samples using TRIzol (TransGen Biotech, Beijing, China). cDNA synthesis for mRNAs and circRNAs was performed with HiScript III RT SuperMix (Vazyme, R323-01), and quantitative PCR was conducted with ChamQ Universal SYBR qPCR Master Mix (Vazyme, Q711-02). For miRNAs, reverse transcription used M-MLV (H-) Reverse Transcriptase (Vazyme, R021-01). Expression levels were normalized to GAPDH (for mRNA/circRNA) or U6 snRNA (for miRNA) using the $2^{-}\Delta\Delta Ct$ method.

$CD8^+$ T cell co-culture

$CD8^+$ T cells were isolated from mouse spleens using MojoSort™ Mouse $CD8^+$ T Cell Isolation Kit (BioLegend, 480007) and activated with anti-

CD3ε/CD28 antibodies (BioLegend, 100339/102115) for 3 days in RPMI-1640 containing IL-2 (10 ng/mL). Lentivirally transfected tumor cells were seeded overnight before coculture with activated T cells at ratios ranging from 1:1 to 1:20. After 48 hours, non-adherent T cells were removed by PBS washing, and the remaining viable tumor cells were quantified using crystal violet staining and OD595 measurements.

Luciferase reporter assays

HEK-293T cells were co-transfected with either wild-type or mutant hsa_circ_0136666, miR-375 mimics or negative control, and wild-type or mutant PRKDC 3′UTR luciferase constructs (pMIR-Report). After 48 hours, luciferase activity was measured using the Duo-Lite Luciferase Assay System (Vazyme) on a microplate reader at 560 nm (Firefly) and 480 nm (Renilla).

RNA-binding protein immunoprecipitation (RIP)

RIP assays were performed using Protein A/G Agarose Resin (Bimake, USA). MKN-45 cells were harvested 48 hours post-transfection with relevant constructs and lysed in NP-40 buffer (Beyotime, China). Lysates were incubated with AGO2 antibody-conjugated beads for 3 hours at 4 °C. RNAs bound to AGO2 were extracted and analyzed by QRT-PCR to confirm interactions.

Cell viability assay (CCK-8)

Cell proliferation was measured using the Cell Counting Kit-8 (CCK-8, Target Mol, USA). MKN-45 and AGS cells were transfected with either hsa_circ_0136666 plasmids or corresponding siRNAs using jetPRIME. Cells were seeded at 2,000 cells per well in 96-well plates with 100 µL of culture medium and incubated for 24 h at 37 °C with 5% CO_2. Subsequently, 10 µL of CCK-8 solution was added to each well, and plates were incubated for an additional 1 h. Absorbance at 450 nm was measured using a microplate reader to determine cell viability.

Western blotting and co-immunoprecipitation

Proteins were extracted using RIPA buffer (EpiZyme, Shanghai, China) and quantified with the BCA Protein Assay Kit (YEASEN, China). SDS-PAGE gels were prepared using the PAGE Gel Fast Preparation Kit (EpiZyme, Shanghai, China). Proteins were transferred to membranes and incubated with primary antibodies overnight at 4 °C. For co-immunoprecipitation, protein lysates were incubated with specific antibodies and Protein A/G beads, followed by detection using standard western blotting procedures.

Enzyme-linked immunosorbent assay (ELISA)

Tumor tissues from mice were weighed and homogenized in saline at a ratio of 1 mg tissue to 9 µL buffer under ice-cold conditions. Levels of IL-6, TGF-β1, and IFN-γ were quantified using mouse-specific ELISA kits (Multiscience) according to the manufacturer's instructions. Standard curves were generated using linear regression for accurate quantification.

siRNA preparation and lipid nanoparticle (LNP) encapsulation

siRNAs targeting hsa_circ_0136666 were synthesized by Biomics and encapsulated in lipid nanoparticles. Lipid components (ionizable lipid: DSPC: cholesterol: PEG-lipid) were dissolved in ethanol at molar ratios of 50:10:38.5:1.5. The lipid mixture was mixed with a 10 mM citrate buffer (pH 4.0) containing siRNA at a volume ratio of 1:3 using a NanoAssembler system (Suzhou Wenhao Microfluidic Technology, China). Formulations were concentrated by ultrafiltration using Amicon Ultra-15 units.

Animal models and treatment protocols

C57BL/c or BALB/c nude mice were subcutaneously injected with tumor cells. Treatments commenced when tumor volumes reached approximately 100 mm^3. Anti-mouse PD-L1 monoclonal antibody was administered intraperitoneally at 2 mg/kg every three days. LNP-encapsulated siRNA was delivered intratumorally at a dose of 40 µg per mouse in ≤100 µL per injection. For combination treatments, dosing was staggered with PD-L1 inhibitors, following the general protocol for subcutaneous xenograft models.

Flow cytometry of tumor-infiltrating cells

Tumors were excised from euthanized mice, cut into small fragments, and digested with 0.25% trypsin for 10–20 minutes. Single-cell suspensions were filtered through 300-mesh nylon meshes and adjusted to 5×10^5 cells/mL. Cells were stained with fluorescently labeled antibodies for 20 minutes at room temperature following standard protocols and analyzed using a BD FACS Celesta cytometer. Data were processed with FlowJo software (V10).

Statistical analysis

All experiments were performed at least three times independently unless stated otherwise. Data are presented as mean ± SD. Statistical comparisons were conducted using unpaired Student's t-test with SigmaPlot 12.0. Significance was denoted as *P ≤ 0.05, **P ≤ 0.01, ***P ≤ 0.001, ****P ≤ 0.0001. Graphs were generated using GraphPad Prism (v8.3.0) or FlowJo (V10).

Results and Discussion

Hsa_circ_0136666 interacts with miR-375 and promotes gastric cancer growth

Our prior research established that miR-375 suppresses gastric cancer progression. Overexpression of miR-375 was found to induce abnormal expression of various long non-coding RNAs, including circRNAs, suggesting the presence of upstream regulators of endogenous miR-375. To identify circRNAs that could act as miR-375 sponges, we analyzed differentially expressed circRNAs in the Gene Expression Omnibus (GEO) dataset GSE147698. A total of 1,466 circRNAs were differentially expressed (P < 0.05, FC > 1.2), of which 1,262 were upregulated **(Figure 1a).**

We further screened these candidates for potential miR-375 binding sites using the ENCORI database (rnasysu.com/encori/index.php). Both circPRKDC and PRKDC contained predicted miR-375 binding sites; however, hsa_circ_0136666 was the only circPRKDC isoform predicted to bind miR-375. This isoform, located at chr8:48,715,866–48,730,122, arises from the circularization of exon 68 to exon 70 of the PRKDC gene, forming a 477-nt circular RNA via back-splicing **(Figure 1b).** Divergent primers were designed to amplify the back-splice junction, and Sanger sequencing of PCR products confirmed the presence of hsa_circ_0136666 in gastric cancer cells **(Figure 1c).**

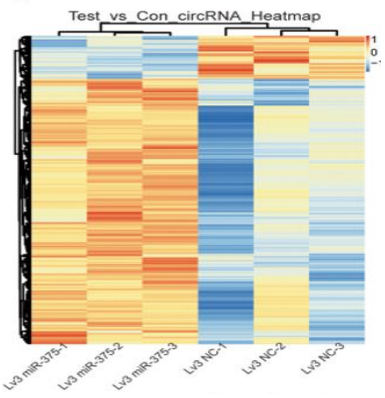

a)

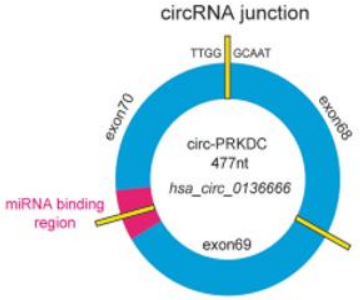

b)

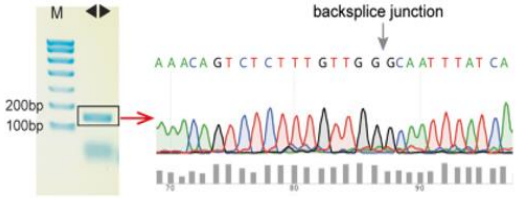

c)

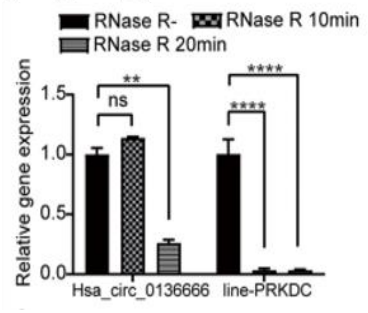

d)

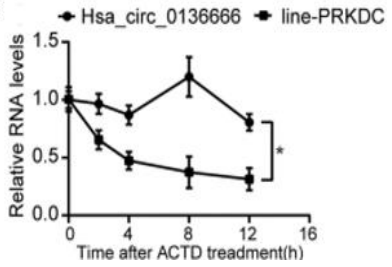

e)

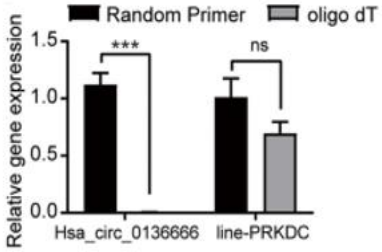

f)

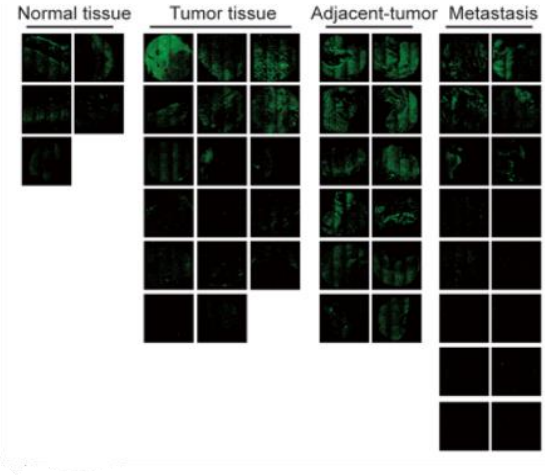

g)

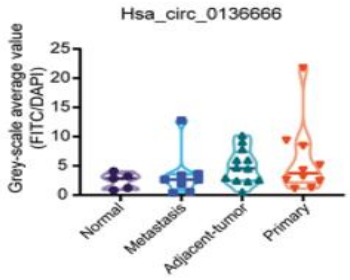

h)

Figure 1. Hsa_circ_0136666 interacts with miR-375 and contributes to gastric cancer progression. (a) Hsa_circ_0136666 is enriched among differentially expressed genes in gene expression profiling. (b) Diagram illustrating the biogenesis of hsa_circ_0136666. (c) Divergent primers amplified the back-splice junction, confirmed by Sanger sequencing. (d) Resistance of hsa_circ_0136666 to RNase R digestion compared with linear PRKDC (n = 3). (e) RNA stability under Actinomycin D treatment showing slower decay of hsa_circ_0136666 relative to linear PRKDC (n = 3). (f) Amplification using oligo dT versus random primers confirmed the lack of poly(A) tail in hsa_circ_0136666 (n = 3). (g) FITC-labeled probes revealed widespread distribution of hsa_circ_0136666 in gastric cancer tissues. (h) Quantification of hsa_circ_0136666 expression across normal, carcinoma in situ, paracancerous, and metastatic tissues. Data are presented as mean ± SD; Student's t-test was used (*P < 0.05, **P < 0.01, ***P < 0.001, ****P < 0.0001).

To confirm its circular structure, RNase R treatment was performed, which preferentially degraded linear PRKDC RNA while leaving hsa_circ_0136666 largely intact **(Figure 1d).** Likewise, under Actinomycin D treatment, hsa_circ_0136666 exhibited prolonged stability compared with its linear counterpart **(Figure 1e).** Amplification with oligo dT primers failed to detect hsa_circ_0136666, confirming its non-polyadenylated circular nature **(Figure 1f)**. Collectively, these results indicate that hsa_circ_0136666 forms a highly stable circular RNA.

FISH analysis demonstrated that hsa_circ_0136666 is expressed broadly across gastric cancer tissues, with highest levels in carcinoma in situ, followed by paracancerous and metastatic tissues, whereas normal gastric tissue exhibited minimal expression **(Figures 1g–1h)**. TCGA analysis revealed that higher miR-375 levels were associated with improved patient survival, while elevated PRKDC expression correlated with poorer outcomes.

These findings suggest that hsa_circ_0136666 is a stable circRNA highly expressed in gastric cancer and likely plays a key regulatory role in tumor progression.

Hsa_circ_0136666 promotes tumor proliferation and immune evasion

Hsa_circ_0136666 expression was consistently elevated across gastric cancer tissues and cell lines, whereas the normal gastric epithelial cell line GES-1 showed minimal expression **(Figure 2a),** indicating tumor-specific overexpression and suggesting a potential role in cancer proliferation and immune escape.

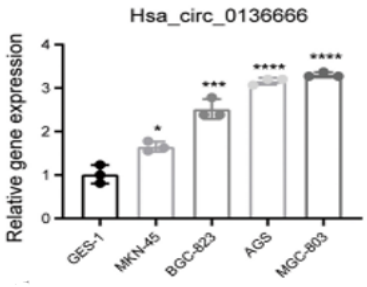

a)

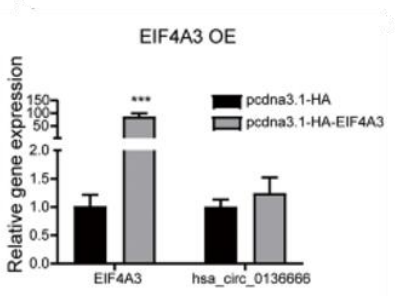

b)

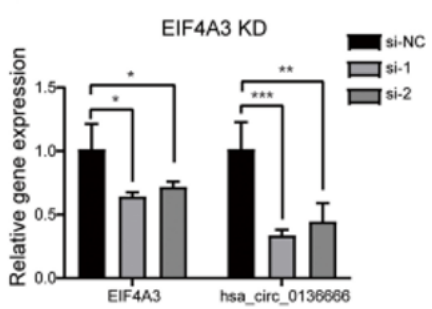
EIF4A3 KD
si-NC
si-1
si-2
Relative gene expression
EIF4A3
hsa_circ_0136666

c)

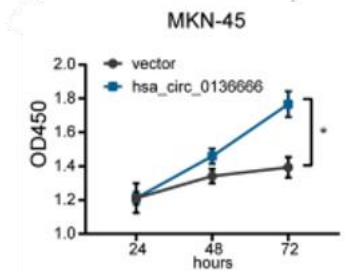
MKN-45
vector
hsa_circ_0136666
OD450
hours

d)

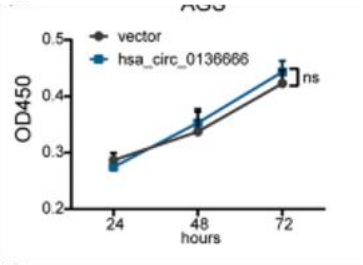
vector
hsa_circ_0136666
OD450
ns
hours

e)

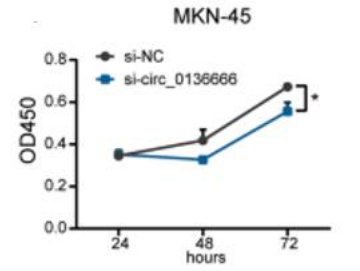
MKN-45
si-NC
si-circ_0136666
OD450
hours

f)

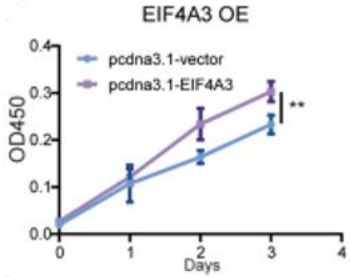
EIF4A3 OE
pcdna3.1-vector
pcdna3.1-EIF4A3
OD450
Days

g)

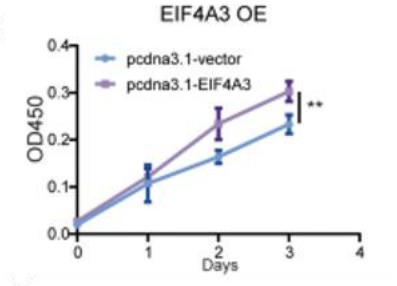
EIF4A3 OE
pcdna3.1-vector
pcdna3.1-EIF4A3
OD450
Days

h)

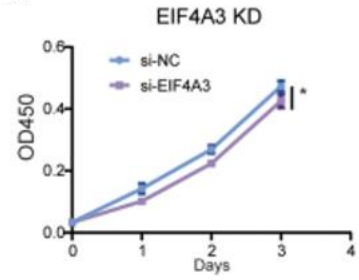
EIF4A3 KD
si-NC
si-EIF4A3
OD450
Days

i)

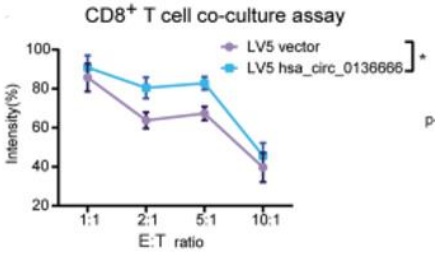
CD8+ T cell co-culture assay
LV5 vector
LV5 hsa_circ_0136666
Intensity(%)
E:T ratio

j)

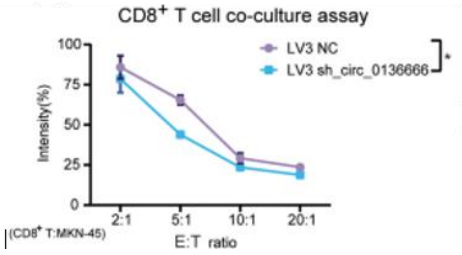
CD8+ T cell co-culture assay
LV3 NC
LV3 sh_circ_0136666
Intensity(%)
E:T ratio

k)

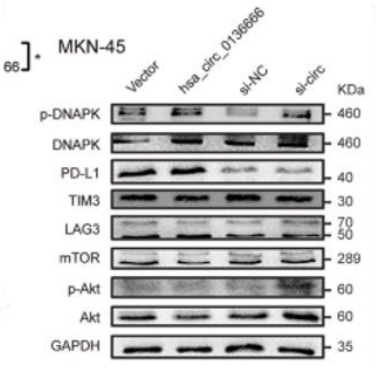
MKN-45
Vector
hsa_circ_0136666
si-NC
si-circ
KDa
p-DNAPK
DNAPK
PD-L1
TIM3
LAG3
mTOR
p-Akt
Akt
GAPDH

l

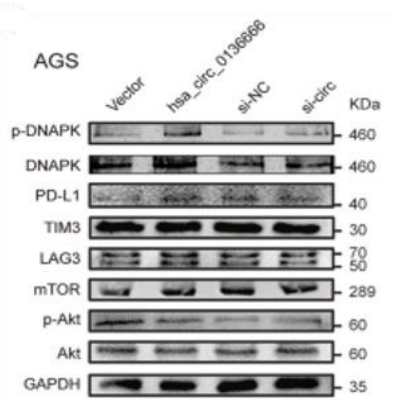

m)

Figure 2. Hsa_circ_0136666 drives tumor proliferation and immune evasion.

(a) Expression levels of hsa_circ_0136666 across various gastric cancer cell lines compared to the normal gastric epithelial cell line GES-1. (b–c) Overexpression or knockdown of EIF4A3 significantly altered hsa_circ_0136666 abundance. (d–g) Cell proliferation assays demonstrated that overexpression of hsa_circ_0136666 enhanced proliferation in MKN-45 and AGS cells, whereas knockdown suppressed growth. (h–i) EIF4A3 overexpression promoted, while its knockdown inhibited, MKN-45 cell proliferation. (j–k) Co-culture with CD8+ T cells revealed increased survival of hsa_circ_0136666-overexpressing tumor cells, reversed by knockdown (n = 6). (l–m) Western blot analysis of immune checkpoint proteins and PI3K pathway components in MKN-45 and AGS cells. Data are mean ± SD (n = 3 unless specified); Student's t-test: *P < 0.05, **P < 0.01, ***P < 0.001, ****P < 0.0001.

EIF4A3, a core component of the exon junction complex essential for pre-mRNA splicing, has been reported to regulate circRNA biogenesis [23]. Analysis using the Circular RNA Interactome indicated four EIF4A3 binding sites flanking the hsa_circ_0136666 pre-mRNA. Consistent with this, qRT-PCR experiments showed that EIF4A3 overexpression increased hsa_circ_0136666 levels, whereas EIF4A3 knockdown reduced its expression in gastric cancer cells **(Figures 2b–c).**

Functional assays demonstrated that hsa_circ_0136666 promotes gastric cancer cell proliferation. CCK-8 assays confirmed that its overexpression enhanced growth in MKN-45 and AGS cells (**Figures 2d and 2e),** while siRNA-mediated knockdown inhibited proliferation **(Figures 2f and 2g)**. Similarly, EIF4A3 overexpression accelerated cell growth, whereas its knockdown impeded proliferation **(Figures 2h and 2i)**, indicating that EIF4A3-dependent biogenesis of hsa_circ_0136666 contributes to tumor growth.

Gene Ontology (GO) analysis of genes negatively correlated with miR-375 in GSE147698 revealed enrichment in signal transduction, immune response, and inflammatory processes, and KEGG pathway analysis highlighted the T cell receptor signaling pathway. Given that PRKDC mutations have been associated with enhanced immunotherapy responses [24], we explored immune regulation by hsa_circ_0136666. Co-culture experiments with activated CD8+ T cells showed that overexpression of hsa_circ_0136666 increased tumor cell survival, whereas knockdown restored susceptibility to T cell-mediated killing **(Figures 2j and 2k)**, suggesting that hsa_circ_0136666 confers resistance to anti-tumor immunity.

Because immune checkpoint blockade is a cornerstone of cancer immunotherapy, we assessed checkpoint-related proteins. Hsa_circ_0136666 overexpression markedly increased PD-L1 levels and other immune checkpoint proteins, while siRNA knockdown reduced PD-L1 expression **(Figures 2l and 2m)**. Notably, hsa_circ_0136666 did not significantly alter mRNA levels of these genes, indicating post-transcriptional regulation.

Collectively, these findings demonstrate that hsa_circ_0136666 promotes gastric cancer cell proliferation while enabling immune evasion, with its biogenesis controlled by EIF4A3.

Hsa_circ_0136666 promotes immune evasion in gastric cancer

To investigate the role of hsa_circ_0136666 in antitumor immunity, murine gastric cancer cells were used to establish a homologous tumor transplantation model. C57BL/6 mice inoculated with MFC cells overexpressing hsa_circ_0136666 exhibited accelerated tumor growth (**Figure 3a)** and increased tumor weight **(Figures 3b and 3c).** Similar results were observed in a BALB/c nude mouse model, confirming that hsa_circ_0136666 enhances tumor progression in vivo.

Given the critical role of the tumor immune microenvironment (TME) in regulating antitumor responses, we next examined whether hsa_circ_0136666 influences immune cell infiltration. Flow cytometry analysis revealed that overexpression of hsa_circ_0136666 significantly reduced the overall number of tumor-infiltrating T cells, while promoting

polarization of tumor-associated macrophages toward the immunosuppressive M2 phenotype **(Figures 3d and 3e)**. Additionally, the populations of myeloid-derived suppressor cells (MDSCs) and regulatory T cells (Tregs) were increased in tumors overexpressing hsa_circ_0136666 **(Figures 3f and 3g)**.

The stable overexpression of hsa_circ_0136666 in the MFC cell model was confirmed **(Figure 3h)**, validating the experimental system. Collectively, these findings indicate that hsa_circ_0136666 not only accelerates tumor growth but also reshapes the TME toward an immunosuppressive state, thereby facilitating immune escape and supporting malignant progression.

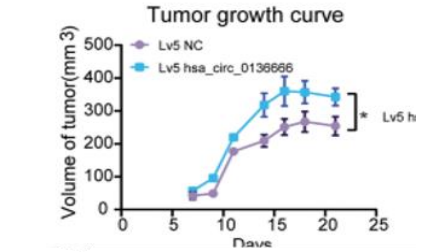

a)

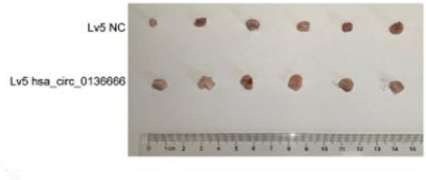

b)

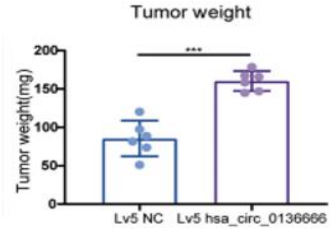

c)

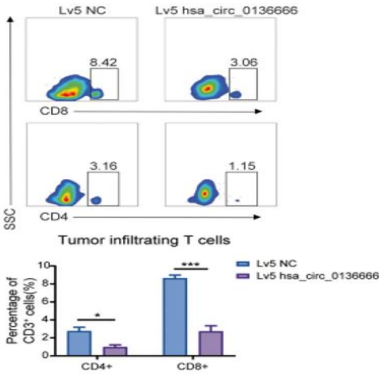

d)

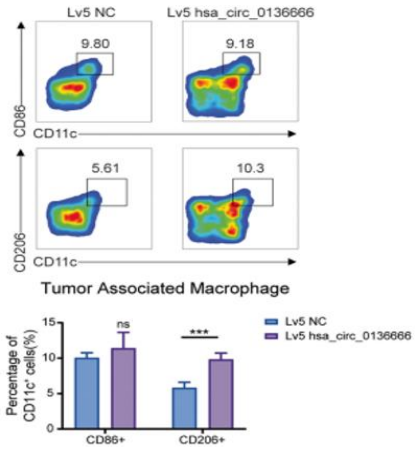

e)

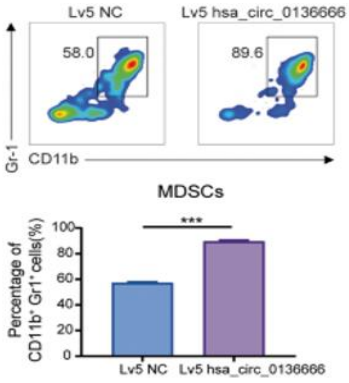

f)

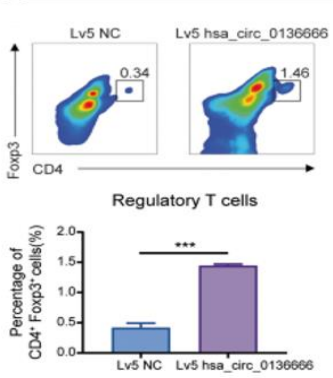

g)

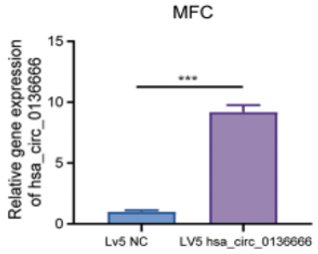

h)

Figure 3. Hsa_circ_0136666 promotes immune escape in gastric cancer.

(a) Tumor growth curves of mice injected with Lv5 MFC cells overexpressing hsa_circ_0136666. (b) Representative images of excised tumors. (c) Comparison of tumor weights. (d–g) Flow cytometry analysis showing differences in tumor-infiltrating T lymphocytes, tumor-associated macrophages, MDSCs, and regulatory T cells. Data are presented as mean ± SD (n = 6); Student's t-test: *P < 0.05, ***P < 0.001. (h) Confirmation of stable hsa_circ_0136666 overexpression in MFC cells (***P < 0.001).

Cytokines are crucial modulators of the tumor immune microenvironment. For instance, TGF-β restricts T cell infiltration, suppressing antitumor immunity [25]. PD-1 blockade induces IFN-γ-mediated YAP aggregation in tumor cells, forming transcriptional hubs that enhance immunosuppressive gene expression and adaptive resistance [26]. Similarly, the IL-6/STAT3 pathway promotes expansion of immunosuppressive cells and alters T cell subset balance, with IL-6 inhibition shown to enhance anti-PD-L1 therapy [27, 20]. In tumors overexpressing hsa_circ_0136666, IFN-γ and IL-6 levels were elevated, whereas TGF-β remained unchanged. Conversely, knockdown of hsa_circ_0136666 reduced these pro-tumorigenic factors. Immunohistochemistry of tumor sections confirmed enhanced local malignancy and elevated PD-L1 expression. These data indicate that hsa_circ_0136666 accelerates tumor growth and contributes to formation of an immunosuppressive microenvironment in vivo.

Hsa_circ_0136666 functions as a miR-375 sponge to promote gastric cancer progression

Previous studies demonstrated that miR-375 suppresses gastric carcinogenesis, including H. pylori-induced inflammation, by modulating immune cell differentiation and cytokine levels. In line with this, hsa_circ_0136666 expression was negatively correlated with miR-375 levels in gastric cancer **(Figure 4a)**. Bioinformatic analysis using starBase v2.0 (http://starbase.sysu.edu.cn/starbase2) predicted potential binding sites between hsa_circ_0136666 and miR-375 **(Figure 4b).**

RNA immunoprecipitation (RIP) assays confirmed this interaction, showing that anti-AGO2 antibody could pull down miR-375 bound to wild-type hsa_circ_0136666 **(Figure 4c)**. Dual-luciferase reporter assays further validated the direct binding, as mutating the predicted binding site abolished the interaction **(Figure 4d)**. These findings indicate that hsa_circ_0136666 acts as a molecular sponge for miR-375, thereby influencing downstream signaling pathways involved in gastric cancer progression.

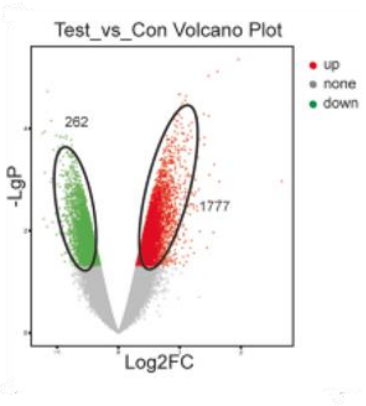

a)

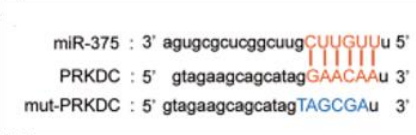

b)

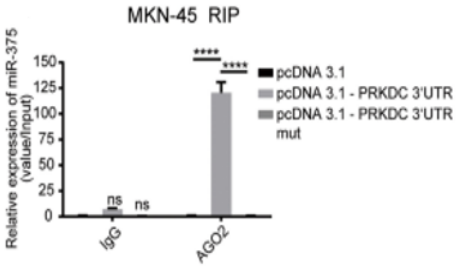

c)

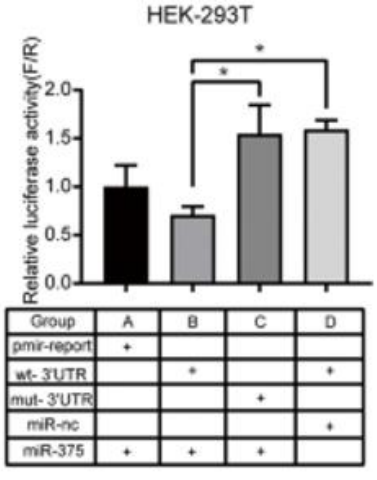

d)

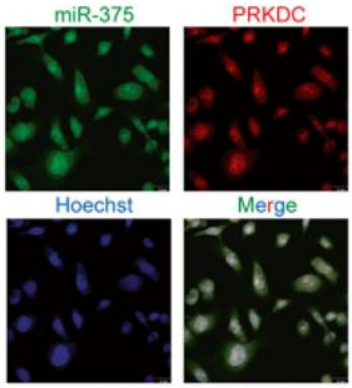

e)

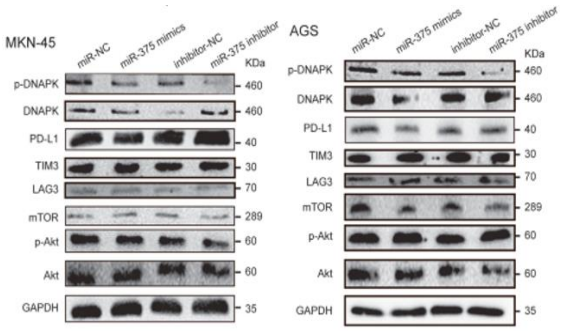

f)

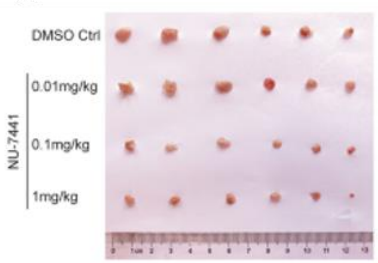

g)

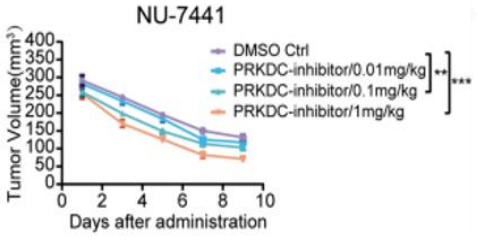

h)

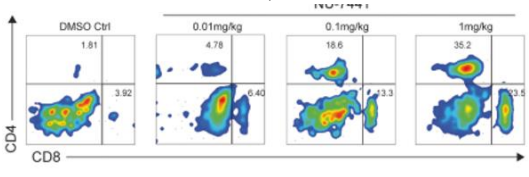

i)

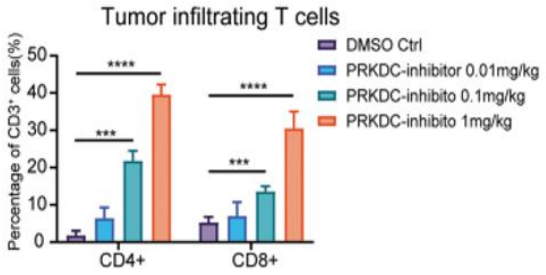

j)

Figure 5. Hsa_circ_0136666 modulates immune responses via the miR-375/PRKDC axis. (a) Microarray analysis of miR-375-overexpressing cells showing 1,777 upregulated and 262 downregulated genes. (b) Predicted complementary binding sites between miR-375 and the PRKDC 3′UTR. (c) RIP assay confirming the interaction between miR-375 and PRKDC mRNA (n = 3). (d) Dual-luciferase reporter assay validating binding, lost upon mutation (n = 6). (e) RNA FISH showing cytoplasmic colocalization of PRKDC mRNA and miR-375. (f) Western blot of immune checkpoint and PI3K pathway proteins in MKN-45 cells following miR-375 overexpression. (g–h) Representative images and tumor growth curves in NU-7441-treated tumor-bearing mice (n = 6). (i–j) Distribution and quantification of tumor-infiltrating T cells under NU-7441 treatment (n = 6). Data are mean ± SD; Student's t-test: *P < 0.05, **P < 0.01, ***P < 0.001, ****P < 0.0001.

FISH analysis revealed that PRKDC mRNA is predominantly cytoplasmic and shows near-complete overlap with miR-375 **(Figure 5e)**. MiR-375, as part of the RISC complex, binds the 3′UTR of PRKDC to inhibit its translation. PRKDC encodes DNA-PKcs, the catalytic subunit of DNA-dependent protein kinase, which forms a Ku70/Ku80 heterodimer critical for DNA double-strand break repair and recombination. Overexpression of miR-375 in MKN-45 and AGS cells reduced PRKDC protein levels, whereas inhibition of miR-375 increased DNA-PK expression **(Figure 5f)**. DNA-PK autophosphorylation reflects its enzymatic activity, and overexpression of hsa_circ_0136666 was associated with increased p-DNA-PK, although this did not reach statistical significance. Notably, DNA-PK modulation had minimal impact on Akt/p-Akt levels, suggesting that hsa_circ_0136666 promotes oncogenesis independently of the Akt/mTOR pathway.

Pharmacological inhibition of DNA-PK using NU-7441 effectively suppressed tumor growth in vivo **(Figures 5g**

and 5h) and enhanced T cell infiltration **(Figures 5i and 5j)**, indicating that blocking DNA-PK reactivates antitumor immunity. These findings support a model in which hsa_circ_0136666 sponges miR-375 to relieve PRKDC repression, allowing DNA-PK to drive tumor progression and facilitate immune evasion.

DNA-PK mediates PD-L1 stabilization via T20/T22 phosphorylation

Prior experiments indicated a close association between PRKDC and PD-L1. We hypothesized that DNA-PK might directly phosphorylate PD-L1, enhancing its protein stability and promoting immune escape. Endogenous co-immunoprecipitation confirmed reciprocal binding between PD-L1 and DNA-PK in tumor cells **(Figure 6a).** In HEK-293T cells overexpressing hsa_circ_0136666 or miR-375 mimics, DNA-PK pull-downs showed increased PD-L1 interaction, consistent with upregulated DNA-PK levels **(Figures 6b and 6c).** Immunofluorescence further demonstrated cytoplasmic colocalization of DNA-PK and PD-L1 **(Figure 6d)**, supporting a direct regulatory mechanism.

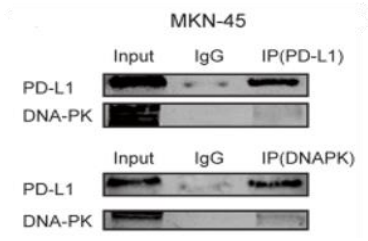

a)

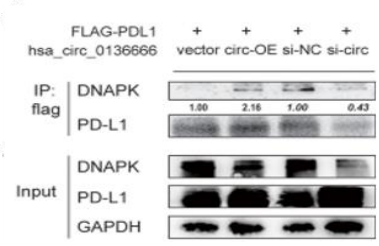

b)

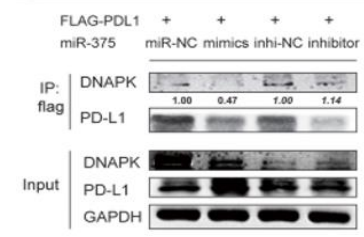

c)

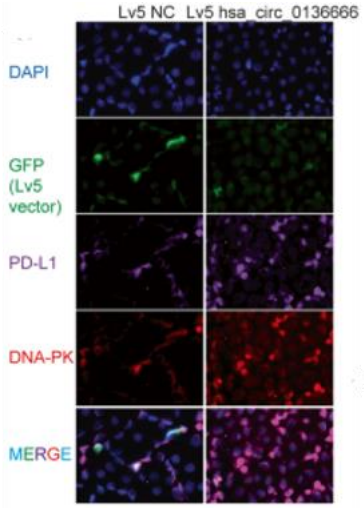

d)

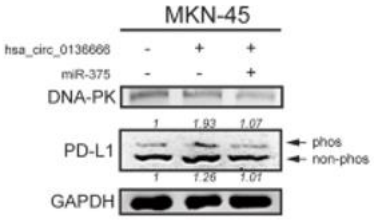

e)

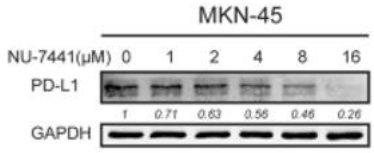

f)

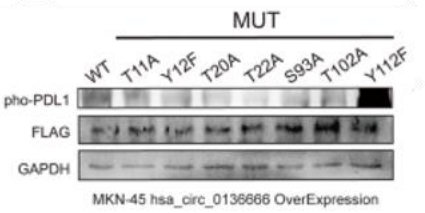

g)

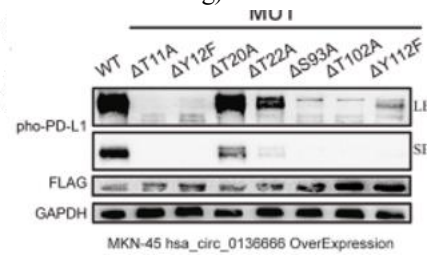

h)

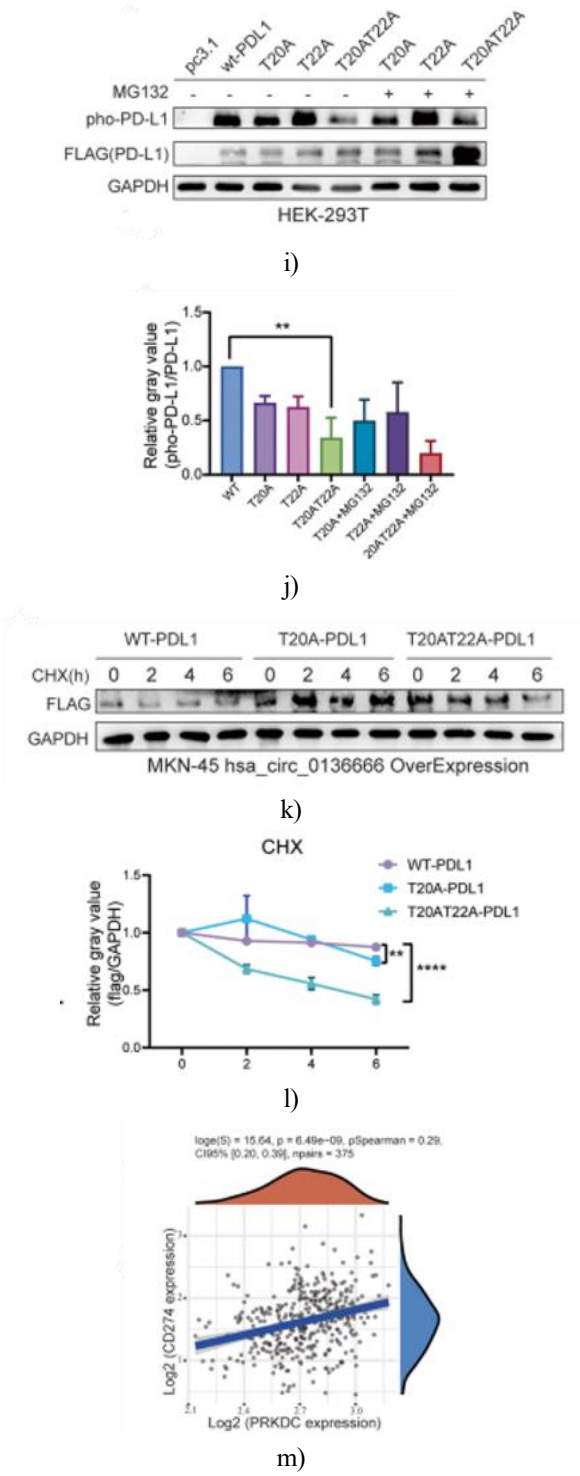

Figure 6. DNA-PK mediates PD-L1 stabilization through dual-site T20/T22 phosphorylation. (a) Endogenous co-immunoprecipitation confirming DNA-PK binding to PD-L1. (b–c) Exogenous co-immunoprecipitation in HEK-293T cells showing DNA-PK interaction with PD-L1 in the presence of hsa_circ_0136666 or miR-375. (d) Immunofluorescence confirming cytoplasmic colocalization of DNA-PK and PD-L1. (e) Rescue experiments using phos-tag SDS-PAGE to detect phosphorylated PD-L1. (f) Concentration-dependent reduction of PD-L1 protein by the DNA-PK inhibitor NU-7441. (g–h) Phosphorylation analysis after single and multiple PD-L1 phosphosite mutations. (i–j) Assessment of PD-L1 phosphorylation after dual-site mutation (T20A/T22A) under MG-132 treatment. (k–l) CHX chase experiments verifying PD-L1 protein stability and quantification. (m) TCGA analysis showing correlation between CD274 (PD-L1) and PRKDC expression. Data are mean ± SD; Student's t-test: $^{**}P < 0.01$, $^{****}P < 0.0001$.

Given that DNA-PK is a member of the PI3K kinase family, we investigated whether it directly phosphorylates PD-L1. Rescue experiments revealed that hsa_circ_0136666 overexpression increased PD-L1 phosphorylation, which was partially reversed by miR-375 **(Figure 6e)**. Inhibition of DNA-PK activity with NU-7441 reduced PD-L1 protein levels in a dose-dependent manner **(Figure 6f).**

Mass spectrometry analysis following DNA-PK immunoprecipitation in HEK-293T cells identified seven potential PD-L1 phosphorylation sites. Phos-tag SDS-PAGE of site-directed mutants revealed that T20 and T22 are critical phosphorylation sites: dual mutation (T20A/T22A) markedly decreased PD-L1 phosphorylation compared with single-site mutants **(Figures 6g-6j).** CHX chase experiments demonstrated that the T20/T22 double mutant exhibited reduced protein stability and accelerated degradation within 6 hours compared with wild-type PD-L1 **(Figures 6k and 6l).** Clinical data from gastric adenocarcinoma samples confirmed a strong positive correlation between PRKDC and PD-L1 expression **(Figure 6m).**

Taken together, these findings indicate that DNA-PK directly interacts with and phosphorylates PD-L1 at T20 and T22, enhancing PD-L1 protein stability, promoting its accumulation, and contributing to immune evasion in gastric cancer.

Hsa_circ_0136666 as a therapeutic target: siRNA enhances anti-PD-L1 efficacy

To evaluate the potential of hsa_circ_0136666 as a therapeutic target, a subcutaneous tumor model was established in C57BL/6 mice **(Figure 7a).** Mice bearing tumors derived from MFC cells overexpressing hsa_circ_0136666 were randomly assigned to four

treatment groups and received intratumoral injections of nanoliposome-encapsulated siRNA (LNP-siRNA; 40 μg per mouse in 100 μL), achieving approximately 50% knockdown efficiency at the cellular level **(Figure 7b)**. In parallel, anti-mouse PD-L1 monoclonal antibody (2 mg/kg) was administered via intraperitoneal injection. Both treatments were repeated every three days.

Tumor growth was markedly suppressed in the LNP-siRNA group compared with control (saline or LNP-siNC). Notably, the combination of LNP-siRNA and anti-PD-L1 therapy further reduced tumor volume relative to anti-PD-L1 monotherapy, with the combination group exhibiting the smallest tumor size and weight among all groups **(Figures 7c–7f).** Tumor inhibition rates were approximately 50–60% compared with controls. Body weights remained stable across all groups, indicating minimal systemic toxicity (**Figure 7d).**

These results suggest that intratumoral delivery of LNP-siRNA effectively targets hsa_circ_0136666, avoiding nuclease-mediated degradation in circulation, and that its combination with anti-PD-L1 therapy synergistically enhances antitumor efficacy.

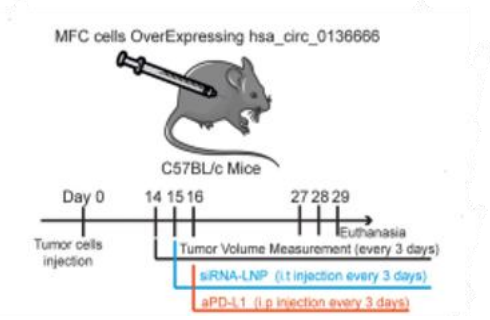

a)

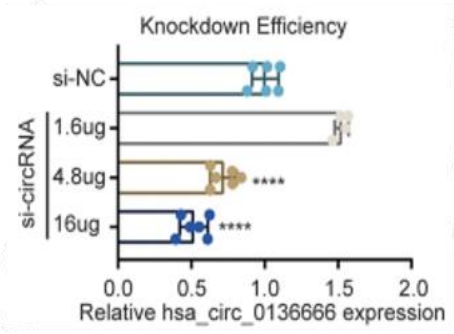

b)

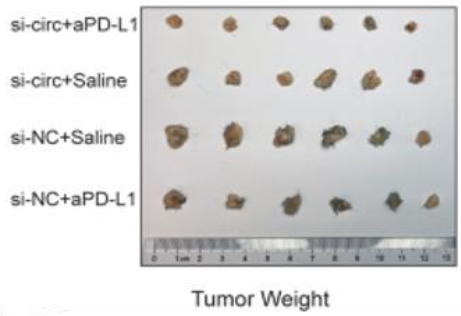

c)

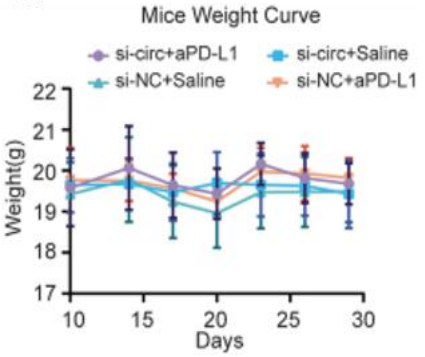

d)

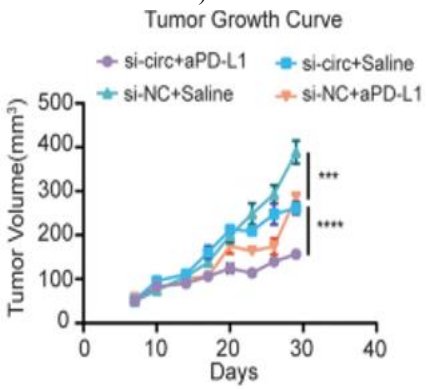

e)

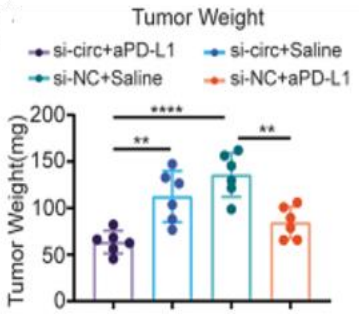

f)

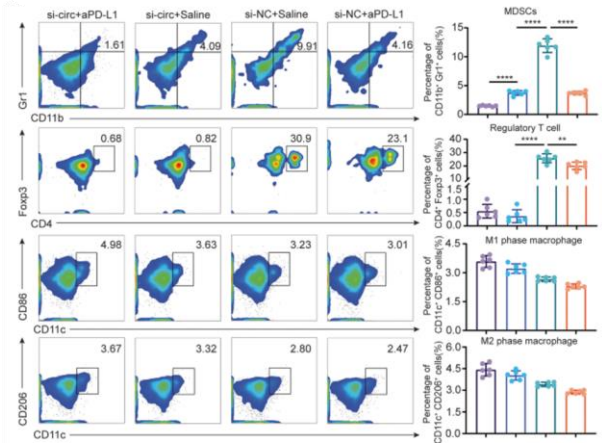

g)

Figure 7. LNP-siRNA targeting hsa_circ_0136666 enhances anti-PD-L1 efficacy and remodels the tumor immune microenvironment**.**

(a) Schematic of dosing regimen: 14 days post-tumor inoculation, mice received intratumoral injections of LNP-siRNA (2 mg/kg) and intraperitoneal injections of anti-PD-L1 antibody (2 mg/kg) on alternating days, repeated every three days for five cycles. (b) qRT-PCR analysis showing siRNA knockdown efficiency (n = 3). (c) Representative tumor images. (d) Body weight curves (n = 6). (e) Tumor growth curves (n = 6). (f) Tumor weight comparisons (n = 6). (g) Distribution and quantification of immunosuppressive cells in tumor tissues (n = 6). Data are mean ± SD; **P < 0.01, ***P < 0.001, ****P < 0.0001.

LNP-siRNA treatment partially inhibited tumor growth, though not as effectively as anti-PD-L1 monotherapy. Importantly, LNP-siRNA significantly modulated the tumor microenvironment by reducing immunosuppressive cell populations. MDSCs were markedly decreased in tumors treated with LNP-siRNA, with the lowest levels observed in the combination group (LNP-siRNA + anti-PD-L1). Similarly, regulatory T cells were reduced in all LNP-siRNA-treated groups, while tumor-associated macrophages showed no significant changes **(Figure 7g).**

Immunofluorescence analysis of tumor-infiltrating CD8+ T cells revealed that the combination treatment group exhibited the highest CD8+ T cell density, accompanied by increased granzyme B expression and the lowest PD-L1 levels. Both LNP-siRNA and anti-PD-L1 monotherapy reduced PD-L1 expression compared with controls.

Overall, these findings demonstrate that LNP-siRNA targeting hsa_circ_0136666 enhances the antitumor efficacy of anti-PD-L1 therapy, suppresses recruitment of immunosuppressive cells, and is well tolerated in vivo, supporting its potential as a safe therapeutic agent.

CircRNAs have emerged as a significant class of noncoding RNAs that contribute to cancer initiation and progression through multiple mechanisms, including miRNA sponging, transcriptional regulation, and interactions with RNA-binding proteins. Recent studies also indicate that some circRNAs can encode short peptides that regulate tumorigenesis. In the case of hsa_circ_0136666, we did not investigate peptide translation because bioinformatic analysis revealed the absence of an internal ribosome entry site (IRES) and a canonical ATG start codon. These features strongly suggest that hsa_circ_0136666 lacks the capacity to produce a functional micropeptide.

CircRNAs have emerged as a significant class of noncoding RNAs that contribute to cancer initiation and progression through multiple mechanisms, including miRNA sponging, transcriptional regulation, and interactions with RNA-binding proteins. Recent studies also indicate that some circRNAs can encode short peptides that regulate tumorigenesis. In the case of hsa_circ_0136666, we did not investigate peptide translation because bioinformatic analysis revealed the absence of an internal ribosome entry site (IRES) and a canonical ATG start codon. These features strongly suggest that hsa_circ_0136666 lacks the capacity to produce a functional micropeptide.

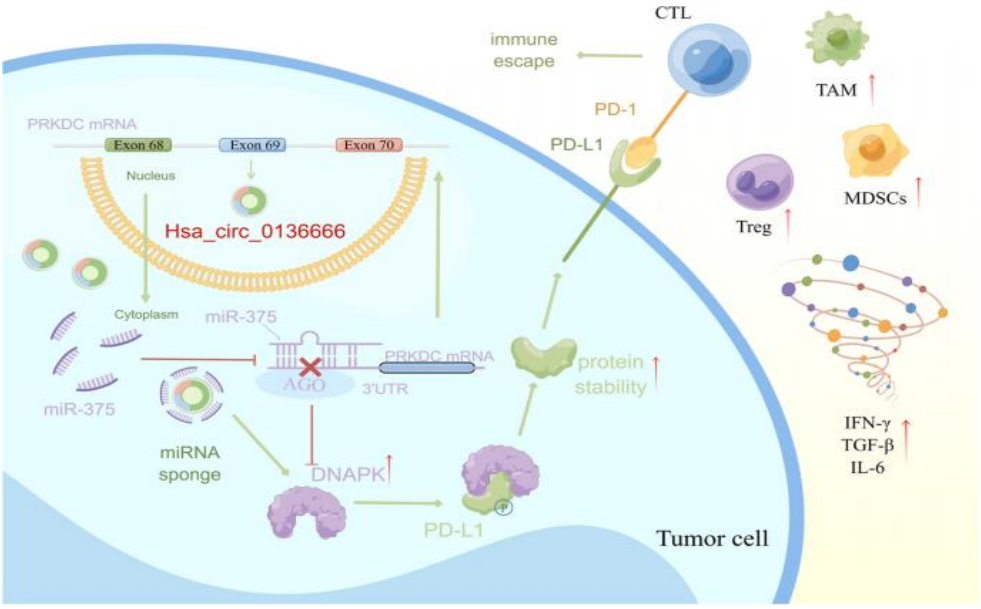

Figure 8. Schematic of the hsa_circ_0136666 signaling pathway in gastric cancer progression.

Hsa_circ_0136666 acts as a miR-375 sponge, leading to upregulation of PRKDC and increased DNA-PK protein levels. DNA-PK phosphorylates PD-L1, enhancing its stability and causing aberrant clustering on the cell membrane, ultimately promoting tumor immune escape.

Small nucleic acid drugs and RNA interference (RNAi) therapeutics

Small nucleic acid drugs, including siRNAs, miRNAs, and antisense oligonucleotides, represent a novel therapeutic class distinct from conventional small molecules or antibodies. Their mechanism relies on sequence-specific gene silencing to inhibit target protein expression, offering potential treatment strategies for diseases driven by elevated gene expression, such as viral infections, cancers, and inflammatory disorders [28–32]. Notably, RNAi technology earned the Nobel Prize in Physiology or Medicine in 2006 for its transformative impact on biomedical research.

Efficient delivery of nucleic acid therapeutics remains a challenge. Naked siRNA exhibits poor in vivo stability due to rapid degradation by nucleases and rapid renal clearance, while its size and negative charge impede cellular uptake. Lipid nanoparticles (LNPs) provide a biocompatible delivery platform that protects siRNA, facilitates cellular uptake, and enhances therapeutic efficacy, representing a promising approach for cancer-targeted therapies, including gastric cancer.

Study limitations

Several limitations should be acknowledged. First, although we focused on hsa_circ_0136666 due to its regulatory relationship with the parental gene PRKDC, other differentially expressed circRNAs were not investigated. Second, we did not explore potential functions of hsa_circ_0136666 beyond miRNA sponging, such as interactions with RNA-binding proteins, and thus cannot attribute its full effect on tumor proliferation and immune escape solely to miR-375 sequestration. Third, the antitumor effect of LNP-siRNA monotherapy was modest, and the combination with anti-PD-L1 therapy only partially enhanced tumor inhibition. As both interventions converge on the PD-L1 axis, broader efficacy may require combination with additional therapeutic agents or humanized mouse models to fully validate clinical potential.

Acknowledgments: We would like to express our gratitude to Dr. Ni for his assistance in the conceptual framework of this study, to Figdraw for the support in the mechanism diagram of this study, and to the Public Experimental Platform of China Pharmaceutical University for assistance in this study.

Conflict of Interest: None

Financial Support: This research was supported by The Priority Academic Program Development (PAPD) of Jiangsu Higher Education Institutions.

Ethics Statement: The study protocol was approved by the Shandong University Research Ethics Committee and Taizhou Hospital Ethics Committee/Shanghai Outdo Biotech Company Ethics Committee. All experimental sections involving human participants in this study were informed and agreed to by the participants.

References

1. Bray F, Ferlay J, Soerjomataram I, Siegel RL, Torre LA, Jemal A. Global cancer statistics 2018: GLOBOCAN estimates of incidence and mortality worldwide for 36 cancers in 185 countries. CA Cancer J Clin. 2018;68:394–424. doi: 10.3322/caac.21492
2. Chen W, Sun K, Zheng R, Zeng H, Zhang S, Xia C, Yang Z, Li H, Zou X, He J. Cancer incidence and mortality in China, 2014. Chin J Cancer Res. 2018;30:1–12. doi: 10.21147/j.issn.1000-9604.2018.01.01
3. Hallinan JT, Venkatesh SK. Gastric carcinoma: imaging diagnosis, staging and assessment of treatment response. Cancer Imaging. 2013;13:212–227. doi: 10.1102/1470-7330.2013.0023
4. Alsina M, Arrazubi V, Diez M, Tabernero J. Current developments in gastric cancer: from molecular profiling to treatment strategy. Nat Rev Gastroenterol Hepatol. 2023;20:155–170. doi: 10.1038/s41575-022-00703-w
5. Zhang XO, Dong R, Zhang Y, Zhang JL, Luo Z, Zhang J, Chen LL, Yang L. Diverse alternative back-splicing and alternative splicing landscape of circular RNAs. Genome Res. 2016;26:1277–1287. doi: 10.1101/gr.202895.115
6. Memczak S, Jens M, Elefsinioti A, Torti F, Krueger J, Rybak A, Maier L, Mackowiak SD, Gregersen LH, Munschauer M, et al. Circular RNAs are a large class of animal RNAs with regulatory potency. Nature. 2013;495:333–338. doi: 10.1038/nature11928
7. Kristensen LS, Andersen MS, Stagsted LVW, Ebbesen KK, Hansen TB, Kjems J. The biogenesis, biology and characterization of circular RNAs. Nat Rev Genet. 2019;20:675–691. doi: 10.1038/s41576-019-0158-7
8. Weng W, Wei Q, Toden S, Yoshida K, Nagasaka T, Fujiwara T, Cai S, Qin H, Ma Y, Goel A. Circular RNA ciRS-7-A Promising Prognostic Biomarker and a Potential Therapeutic Target in Colorectal Cancer. Clin Cancer Res. 2017;23:3918–3928. doi: 10.1158/1078-0432.CCR-16-2541
9. Verduci L, Ferraiuolo M, Sacconi A, Ganci F, Vitale J, Colombo T, Paci P, Strano S, Macino G, Rajewsky N, Blandino G. The oncogenic role of circPVT1 in head and neck squamous cell carcinoma is mediated through the mutant p53/YAP/TEAD transcription-competent complex. Genome Biol. 2017;18:237. doi: 10.1186/s13059-017-1368-y
10. Zhang J, Liu H, Hou L, Wang G, Zhang R, Huang Y, Chen X, Zhu J. Circular RNA_LARP4 inhibits cell proliferation and invasion of gastric cancer by sponging miR-424-5p and regulating LATS1 expression. Mol Cancer. 2017;16:151. doi: 10.1186/s12943-017-0719-3
11. Tang W, Fu K, Sun H, Rong D, Wang H, Cao H. CircRNA microarray profiling identifies a novel circulating biomarker for detection of gastric cancer. Mol Cancer. 2018;17:137. doi: 10.1186/s12943-018-0888-8
12. Thomson DW, Dinger ME. Endogenous microRNA sponges: evidence and controversy. Nat Rev Genet. 2016;17:272–283. doi: 10.1038/nrg.2016.20
13. Saliminejad K, Khorram Khorshid HR, Soleymani Fard S, Ghaffari SH. An overview of microRNAs: Biology, functions, therapeutics, and analysis methods. J Cell Physiol. 2019;234:5451–5465. doi: 10.1002/jcp.27486
14. Ni H, Qin H, Sun C, Liu Y, Ruan G, Guo Q, Xi T, Xing Y, Zheng L. MiR-375 reduces the stemness of gastric cancer cells through triggering ferroptosis. Stem Cell Res Ther. 2021;12:325. doi: 10.1186/s13287-021-02394-7
15. Zhang Z, Chen S, Fan M, Ruan G, Xi T, Zheng L, Guo L, Ye F, Xing Y. Helicobacter pylori induces gastric cancer via down-regulating miR-375 to inhibit dendritic cell maturation. Helicobacter. 2021;26:e12813. doi: 10.1111/hel.12813
16. Abdel-Wahab R, Yap TA, Madison R, Pant S, Cooke M, Wang K, Zhao H, Bekaii-Saab T, Karatas E, Kwong LN, et al. Genomic profiling reveals high frequency of DNA repair genetic aberrations in gallbladder cancer. Sci Rep. 2020;10:22087. doi: 10.1038/s41598-020-77939-6
17. Liiv I, Rebane A, Org T, Saare M, Maslovskaja J, Kisand K, Juronen E, Valmu L, Bottomley MJ,

Kalkkinen N, Peterson P. DNA-PK contributes to the phosphorylation of AIRE: importance in transcriptional activity. Biochim Biophys Acta. 2008;1783:74–83. doi: 10.1016/j.bbamcr.2007.09.003

18. Wang Y, Sun Q, Mu N, Sun X, Wang Y, Fan S, Su L, Liu X. The deubiquitinase USP22 regulates PD-L1 degradation in human cancer cells. Cell Commun Signal. 2020;18:112. doi: 10.1186/s12964-020-00612-y
19. Yao H, Lan J, Li C, Shi H, Brosseau JP, Wang H, Lu H, Fang C, Zhang Y, Liang L, et al. Inhibiting PD-L1 palmitoylation enhances T-cell immune responses against tumours. Nat Biomed Eng. 2019;3:306–317. doi: 10.1038/s41551-019-0375-6
20. Chan LC, Li CW, Xia W, Hsu JM, Lee HH, Cha JH, Wang HL, Yang WH, Yen EY, Chang WC, et al. IL-6/JAK1 pathway drives PD-L1 Y112 phosphorylation to promote cancer immune evasion. J Clin Invest. 2019;129:3324–3338. doi: 10.1172/JCI126022
21. Wang X, Teng F, Kong L, Yu J. PD-L1 expression in human cancers and its association with clinical outcomes. Onco Targets Ther. 2016;9:5023–5039. doi: 10.2147/OTT.S105862
22. Wu B, Song M, Dong Q, Xiang G, Li J, Ma X, Wei F. UBR5 promotes tumor immune evasion through enhancing IFN-gamma-induced PDL1 transcription in triple negative breast cancer. Theranostics. 2022;12:5086–5102. doi: 10.7150/thno.74989
23. Liu Y, Ma L, Hua F, Min Z, Zhan Y, Zhang W, Yao J. Exosomal circCARM1 from spheroids reprograms cell metabolism by regulating PFKFB2 in breast cancer. Oncogene. 2022;41:2012–2025. doi: 10.1038/s41388-021-02061-4
24. Tan KT, Yeh CN, Chang YC, Cheng JH, Fang WL, Yeh YC, Wang YC, Hsu DS, Wu CE, Lai JI, et al. PRKDC: new biomarker and drug target for checkpoint blockade immunotherapy. J Immunother Cancer. 2020;8(1):e000485.
25. Mariathasan S, Turley SJ, Nickles D, Castiglioni A, Yuen K, Wang Y, Kadel EE, III, Koeppen H, Astarita JL, Cubas R, et al. TGFbeta attenuates tumour response to PD-L1 blockade by contributing to exclusion of T cells. Nature. 2018;554:544–548. doi: 10.1038/nature25501
26. Yu M, Peng Z, Qin M, Liu Y, Wang J, Zhang C, Lin J, Dong T, Wang L, Li S, et al. Interferon-gamma induces tumor resistance to anti-PD-1 immunotherapy by promoting YAP phase separation. Mol Cell. 2021;81(1216–1230):e1219. doi: 10.1016/j.molcel.2021.01.010
27. Mace TA, Shakya R, Pitarresi JR, Swanson B, McQuinn CW, Loftus S, Nordquist E, Cruz-Monserrate Z, Yu L, Young G, et al. IL-6 and PD-L1 antibody blockade combination therapy reduces tumour progression in murine models of pancreatic cancer. Gut. 2018;67:320–332. doi: 10.1136/gutjnl-2016-311585
28. Downward J. RNA interference. BMJ. 2004;328:1245–1248. doi: 10.1136/bmj.328.7450.1245
29. Damm-Welk C, Fuchs U, Wossmann W, Borkhardt A. Targeting oncogenic fusion genes in leukemias and lymphomas by RNA interference. Semin Cancer Biol. 2003;13:283–292. doi: 10.1016/S1044-579X(03)00042-7
30. Ge Q, McManus MT, Nguyen T, Shen CH, Sharp PA, Eisen HN, Chen J. RNA interference of influenza virus production by directly targeting mRNA for degradation and indirectly inhibiting all viral RNA transcription. Proc Natl Acad Sci U S A. 2003;100:2718–2723. doi: 10.1073/pnas.0437841100
31. Gitlin L, Karelsky S, Andino R. Short interfering RNA confers intracellular antiviral immunity in human cells. Nature. 2002;418:430–434. doi: 10.1038/nature00873
32. Coburn GA, Cullen BR. Potent and specific inhibition of human immunodeficiency virus type 1 replication by RNA interference. J Virol. 2002;76:9225–9231. doi: 10.1128/JVI.76.18.9225-9231.2002